INORGANIC CATIONS IN THE CELL NUCLEUS

Selective Accumulation during Meiotic Prophase in Mouse Testis

LAURA L. TRES, A. L. KIERSZENBAUM, and C. J. TANDLER

From the Centro de Investigaciones sobre Reproducción, Facultad de Medicina, and the Instituto de Anatomía General y Embriología, Facultad de Medicina, Buenos Aires, Argentina. Dr. Tres's present address is the Department of Anatomy, Duke University Medical Center, Durham, North Carolina 27706.

ABSTRACT

Earlier reports indicated the presence of significant amounts of inorganic salts in the nucleus. In the present study the possibility that this might be related to the transcription process was tested on seminiferous epithelium of the adult mouse, using potassium pyroantimonate as a fixative. The results indicated that a correlation exists between the inorganic cations comprising the pyroantimonate-precipitable fraction and the RNA synthetic activity. During meiotic prophase an accumulation of cation-antimonate precipitates occurs dispersed through the middle pachytene nuclei, the stage in which RNA synthesis reaches a maximum. At other stages (zygotene to diplotene), where RNA synthesis falls to a low level, that pattern is not seen; cation-antimonate deposits are restricted to a few masses in areas apparently free of chromatin. The condensed sex chromosomes, the heterochromatin of the "basal knobs," the axial elements, and the synaptonemal complexes are devoid of antimonate deposits during the meiotic prophase. The Sertoli cells, active in RNA synthesis in both nucleoplasm and nucleolus, show cation-antimonate deposits at these sites. In the nucleoplasm some "patches" of precipitates appear coincident with clusters of interchromatin granules; in the nucleolus the inorganic cations are mainly located in the fibrillar and/or amorphous areas, whereas relatively few are shown by the granular component. The condensed chromatin bodies associated with the nucleolus were always free of antimonate precipitates. It is suggested that the observed sites of inorganic cation accumulation within the nucleus may at least partially indicate the presence of RNA polymerases, the activity of which is dependent on divalent cations.

INTRODUCTION

A significant concentration of inorganic salts is present in the nucleus (1–3), but the functional significance of this remains to be elucidated. A more accurate knowledge of intranuclear ionic conditions, particularly in response to different cell events, should provide an indication if means were at hand to localize them. A method recently has been developed which allows the visualization of inorganic cations (except K^+) at their cellular and subcellular locations with the electron microscope (4, 5). One constantly observed result was, indeed, the presence of a significant accumulation of inorganic cations (Mg^{++}, Ca^{++}, and Na^+) in the nucleus, the amount and intranuclear distribution of which varied in several tissues. Tandler et al. (6) already observed an apparent correlation between the amount of those inorganic cations and that of the ribonucleoprotein particles.

At present there is increasing evidence (7) that at least three transcription systems exist in eucaryotic nuclei, each controlled by a specific DNA-dependent RNA polymerase occurring at different (nucleolar and nucleoplasmic) locations; their enzymic activity is dependent on a divalent cation—either Mg^{++} or Mn^{++}—and they have different ionic strength optima.

The functional significance of inorganic salt accumulation in the nucleus, therefore, might be related to the transcription process. If this is so, one should find—in a given tissue—a selective, high concentration of inorganic cations in those nuclei engaged in active RNA synthesis. The mouse testis is a favorable material on which to test this hypothesis, since Monesi (8, 9) established the RNA synthetic activity in the seminiferous tubules. In the present paper, we demonstrate that the patterns of intranuclear inorganic cation accumulation indeed can be correlated with sites of RNA synthesis.

MATERIALS AND METHODS

Adult Swiss mice (Rockland strain) were anesthetized with ether. The testes were quickly dissected free, minced into small pieces in a drop of the fixative at room temperature (20°-25°C), and thereafter immersed in a larger amount of the fixative. Some animals were perfused through the epididymis by retrogressive injection of the fixative towards the testis, which was then sliced and afterwards immersed in the fixative.

Electron Microscope Fixation and Staining Procedure

The fixative used was a saturated aqueous solution of potassium pyroantimonate (Riedel-De Häen AG, Seelze, Hanover, Germany, analytical reagent) freshly prepared by boiling the salt in twice glass-distilled water, cooling rapidly to room temperature, and centrifuging (pH about 9.2). After fixation—as described above—the testis was hardened with formaldehyde, postosmicated and washed with three changes of distilled water as described before (4, 5). Afterwards, the tissues were dehydrated with graded concentrations of cold ethanol, passed through propylene oxide, and embedded in Maraglas (The Marblette Company, Div. of Allied Products Corp., Long Island City, N.Y.). Thin (gold-to-purple colored) sections were cut with glass knives on a Porter-Blum microtome, mounted on Formvar-coated copper grids, and examined *unstained* with a Siemens Elmiskop I electron microscope.

Thin sections of pyroantimonate-fixed tissues cannot be stained with the usual uranyl acetate and lead citrate procedures unless the grids are treated with oxalic acid: simultaneous staining and removal of antimonate deposits are obtained, as described previously (5). In the present study, this procedure was modified in that staining also can be achieved almost without removal of antimonate precipitates, by simply lowering the oxalic acid concentration (one volume of a saturated solution in 400 vol of distilled water). Thin sections were immersed in this solution for 10–30 sec, washed with distilled water, and thereafter stained with an aqueous solution of uranyl acetate followed by lead citrate as usual.

The rationale of this procedure probably depends on the fixing action of the pyroantimonate anion which complexes with unidentified reactive tissue groups, blocking the uranyl- and lead-stainable sites (5). Since there is almost no electron opacity (at sites which appear free of precipitate), it was reasoned that the amount of "complexed" pyroantimonate anion must be quite low and might be removed without appreciable solubilization of cation-antimonate precipitates. The fact that the staining properties of these tissues can be restored by such a low concentration of oxalic acid further supports this interpretation. The electron micrographs were always obtained first in the unstained sections in order to be sure that there is no appreciable solubilization of precipitates.

Identification of the atomic elements with the electron microprobe in pyroantimonate-fixed mouse testis has been described previously (4).

Timing of the Meiotic Prophase

Labeling of the spermatogenic stages in pyroantimonate-fixed thin sections is based on the same basic features that were described by Solari (10) after a conventional glutaraldehyde–osmium tetroxide fixation. A thick (1 μ) section also was cut sequentially, fastened to a microscope slide and stained with Unna's polychrome blue; this section was examined with the light microscope and labeled according to Oakberg's classification of the stages of spermatogenesis (11).

RESULTS

In mouse testis the pattern of cation-antimonate precipitation during meiotic prophase was found to be characteristically stage dependent. Figs. 1–10 show that there are at least two main patterns of antimonate deposition: (*a*) clusters of precipitates aggregated at interchromatin areas in nuclei whose chromosomes are relatively free of precipitate, and (*b*) precipitates dispersed over the larger part of the nucleus rather than concentrated in a few loci. The characteristics of the electron-opaque precipitates are similar in all cases, although variations in size are evident.

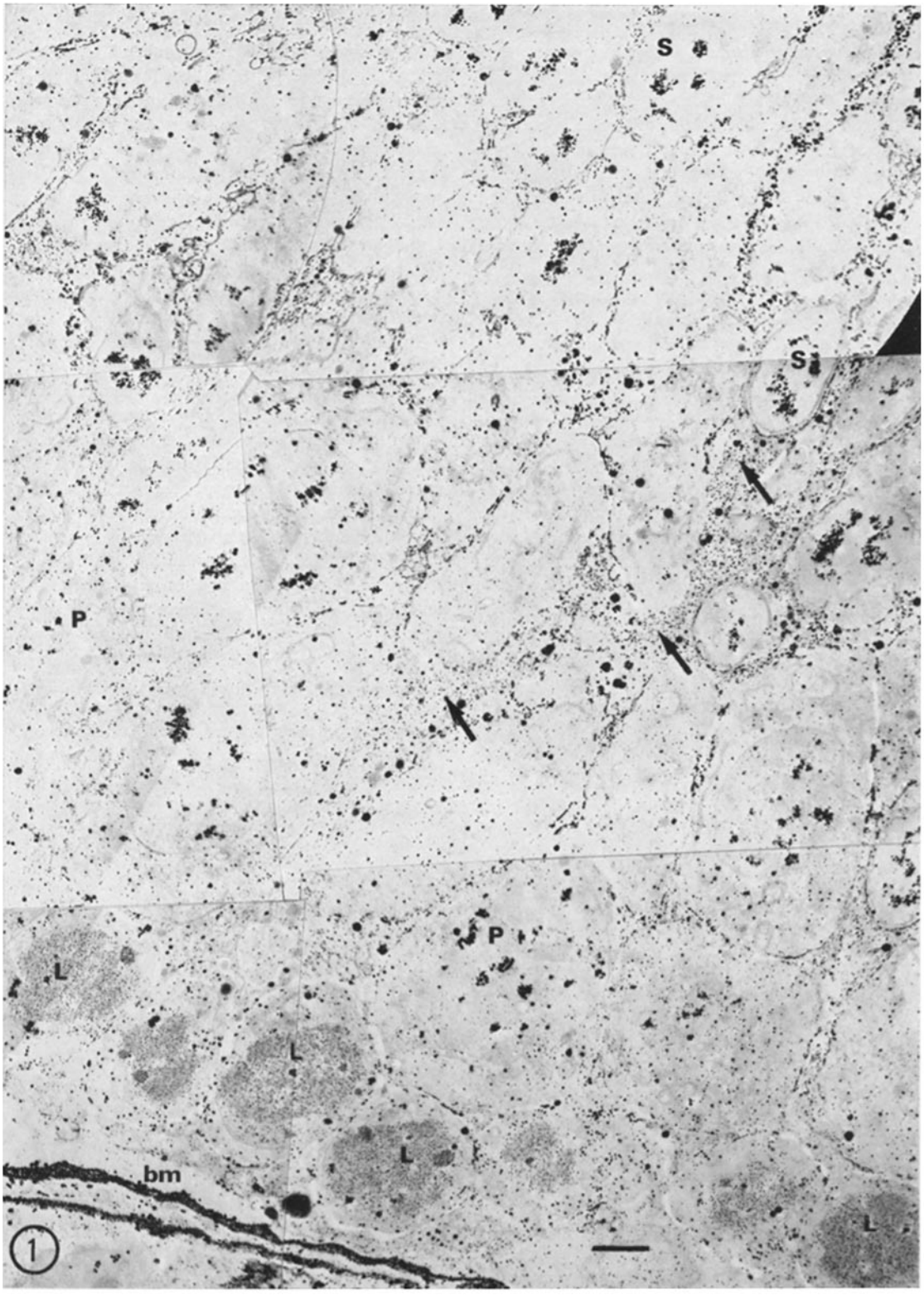

FIGURE 1 Survey electron micrograph of a thin section through a seminiferous tubule (Oakberg's stage IX). The spermatids with elongated nuclei (*S*) are associated with early and late spermatocytes, leptotene (*L*) and late pachytene (*P*); cation-antimonate precipitates are evident in these nuclei. The basal membrane (*bm*) and cytoplasm of Sertoli cells (arrows) show electron-opaque precipitates. Pyroantimonate fixation. Unstained. Scale mark, 4 μ. $\times$ 2350.

The type *a* pattern is shown by zygotene (Fig. 3), early pachytene (Fig. 4), late pachytene (Figs. 1 and 7), and diplotene stages (diakinesis stages were not encountered). According to Monesi (9), there is a low level of RNA synthesis at these stages.

The type *b* pattern corresponds to middle pachytene (Figs, 5 and 6), a stage in which RNA synthesis increases rapidly to a maximum and the autosomal chromosomes show a decondensed appearance (9).

The sex chromosomes, which appear as a chromatin-condensed body (12, 13), are devoid of antimonate deposits during the meiotic prophase (Figs. 4, 6, 7, and 9). The synaptonemal complexes and axial elements are well preserved by pyroantimonate fixation in the whole nucleus and were always free of precipitates (Figs. 3, 4, 8, and 9).

In the cytoplasm, mitochondria usually show the presence of one or a few antimonate deposits (Figs. 5 and 9), very similar in appearance to those described in pyroantimonate-fixed rat kidney (5). In middle pachytene spermatocytes, a few clusters of antimonate precipitates were frequently observed (Fig. 5); owing to their size and frequency, they might correspond to the satellite body (12).

Relationship between Cation-Antimonate Deposits and the Chromosomes

The zygotene stage is easily identified by the condensed appearance of the chromatin, the presence of synaptonemal complexes and axial elements (Fig. 3), as well as by the formation of the sex pair (sex vesicle). Little or no antimonate precipitates were found along the margins of the chromosomes. The pattern of cation-antimonate deposits in the early pachytene nuclei (Fig. 4) is very similar to that of the zygotene stage (i.e., *interchromosomal* localization). The sex pair is now broadly associated with the nuclear membrane; inside its chromatin, several sections of cores and, in some cases, apparently a small synaptonemal complex are observed.

In sections through seminiferous tubules, the late pachytene stages (tubule stages VIII–X) are associated with early spermatocytes (leptotene and zygotene). Their nuclei show the autosomal chromatin to be very decondensed and largely free of antimonate deposits (Figs. 7 and 9); the sex pair remains comparatively more condensed, and the presence of some elements characteristic of the main nucleolus, which is well developed at this stage (10, 14, 15), is now evident.

At middle pachytene stage a large amount of antimonate precipitates is dispersed over the larger part of the nucleus (Figs. 5 and 6), and a few clusters are also seen (Fig. 5). At this stage the chromatin is more decondensed with respect to early pachytene, and areas of condensed chromatin contacting the nuclear envelope ("basal knobs," reference 16) are seen to be free of antimonate precipitates (Figs. 5 and 11). Intermediate types of precipitation pattern, between early and middle

FIGURE 2 Two leptotene spermatocytes showing a fine antimonate precipitate over the chromatin. Basal membrane, *bm*. Pyroantimonate fixation. Unstained. Scale mark, 2 μ. × 7500.

FIGURE 3 Nucleus of a spermatocyte at zygotene stage. Antimonate precipitates are absent from the chromatin, which has a condensed appearance and shows the presence of axial elements (arrow) and synaptonemal complex (↔). Clusters of precipitates are observed in some interchromatin areas. Part of a spermatogonial nucleus is seen at bottom left. Pyroantimonate fixation. Unstained. Scale mark, 1 μ. × 9000.

FIGURE 4 Spermatocyte nucleus at early pachytene. The pattern of antimonate distribution is similar to that of Fig. 3. A secondary nucleolus (*n*) and the heterochromatin of the sex pair (*XY*), which shows an axial element, are free of precipitate. A synaptonemal complex is evident (↔). Pyroantimonate fixation. Unstained. Scale mark, 1 μ. × 13,500.

FIGURE 5 Nucleus of a spermatocyte at middle pachytene stage. A large amount of cation-antimonate precipitates is dispersed over a large part of the nucleus, and a few clusters are also seen. A mass of condensed chromatin with a synaptonemal complex (↔) is free of precipitate. In the cytoplasm the mitochondria (*m*) show a few antimonate deposits; clusters of precipitate are probably related to the satellite body (*b*). Pyroantimonate fixation. Unstained. Scale mark, 1 μ. × 8000.

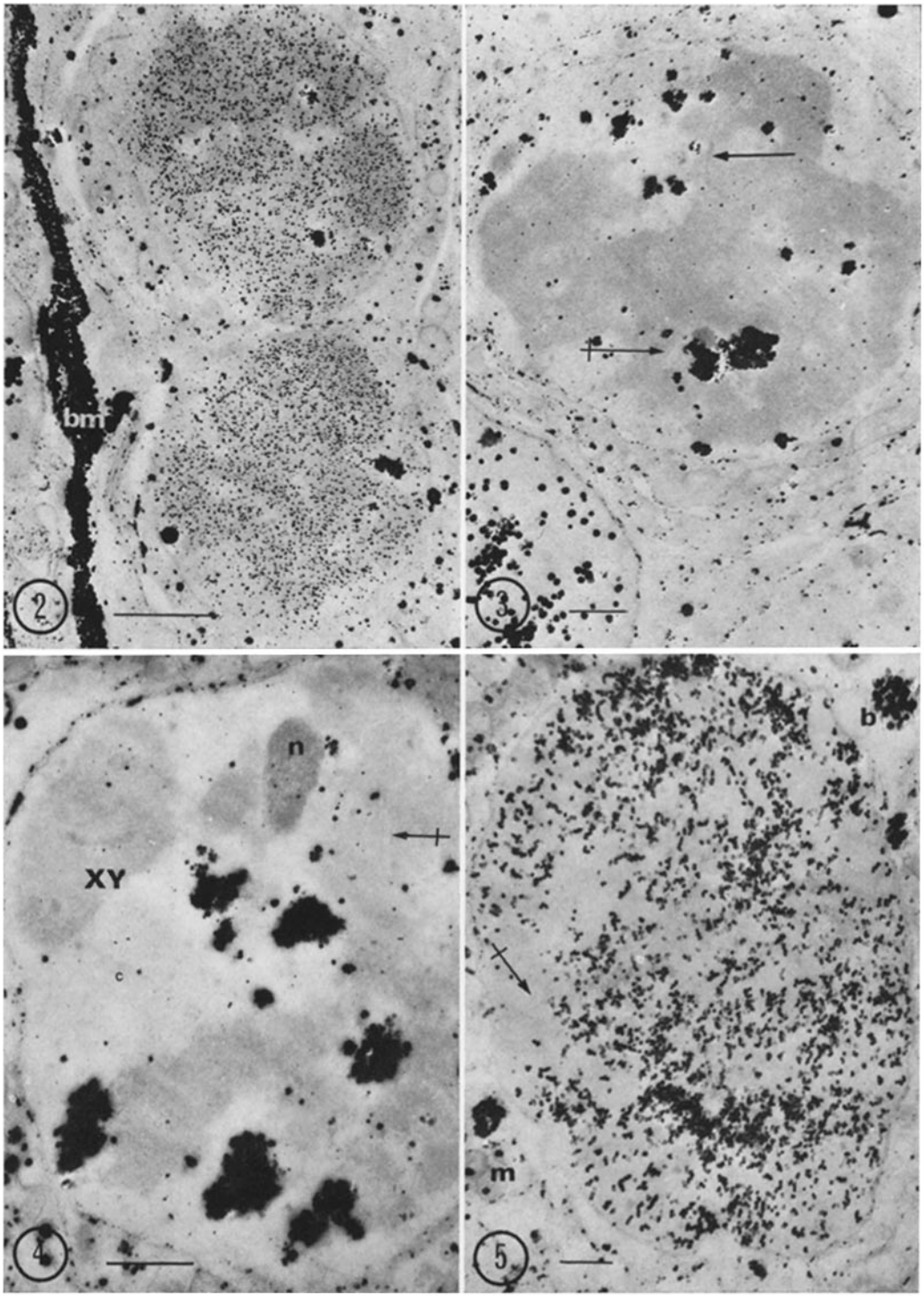
bm
2
3
n
XY
c
4
b
m
5

pachytene stages, indicate that the deposits are frequently located along the margins of autosomal chromatin (Figs. 6 and 10), i.e., *perichromosomal* localization.

A large number of interchromatin and perichromatin granules are evidenced between the autosomal chromatin at middle pachytene, presumably as a result of enhanced RNA synthetic activity; a few clusters of interchromatin granules are also present (Fig. 11). These particles are similar in size and morphology to those described in other mammalian tissues (17–19). The so-called secondary nucleoli (10, 14), which are fully developed at middle pachytene (Fig. 11) and are usually attached to or near the basal knobs, appear relatively free of precipitate (Figs. 4 and 8).

During leptotene (Figs. 1 and 2) the chromatin is "filled" with a finely granular antimonate precipitate. This pattern differs from that given by middle pachytene nuclei. The identification of the leptotene stage is evidenced by the cellular associations (tubule stage IX, Fig. 1). The cells that contain leptotene nuclei form rows of several cells that are at the same stage and are separated from the basement membrane by extensions of the Sertoli cells. Leptotene nuclei are characterized by the beginning of chromatin condensation (Fig. 2); the axial elements are not well discernible from the surrounding chromatin, although they can be distinguished by their longitudinal continuity through the chromosomes (20). Two or three small dense bodies—presumably condensed chromatin—which are closely related to the nuclear membrane also show a fine antimonate precipitate (Fig. 1). It is of interest that although RNA synthesis is relatively low at leptotene (9), DNA synthesis extends into these nuclei (21, 22).

Sertoli Cells

The nuclei of Sertoli cells are very active in RNA synthesis which occurs both in the nucleolus and in the extranucleolar part of the nucleus, whereas no activity is shown by the condensed chromatin bodies associated with the nucleolus (9). From the above-described correlations found for the meiotic nuclei, one should expect a high accumulation of inorganic cations in the nuclei of Sertoli cells. Fig. 12 demonstrates that this is indeed the case: numerous dispersed and aggregated cation-antimonate precipitates are evident in the nucleoplasm. The last type of precipitate apparently corresponds to areas where clusters of interchromatin granules are accumulated, as observed in glutaraldehyde-osmium tetroxide–fixed nuclei (Fig. 13).

A nucleolus also is seen in many pyroantimonate-fixed Sertoli cells (Fig. 12). The cation-antimonate deposits are not evenly distributed in the whole nucleolar body, and two types of precipitates (fine and coarse) are evident; the coarser type of

FIGURE 6 Spermatocyte nucleus at middle pachytene. The distribution of abundant antimonate precipitates along the margins of chromatin is evident. Synaptonemal complex (↔). *XY*, the sex pair with an axial element. Pyroantimonate fixation. Unstained. Scale mark, 2 μ. × 6000.

FIGURE 7 Portion of a late pachytene nucleus showing the sex pair (*XY*) with an associated element of the main nucleolus (arrow). The antimonate precipitates are located in clusters in the rest of the nucleus. Pyroantimonate fixation. Unstained. Scale mark, 2 μ. × 5000.

FIGURE 8 The autosomal chromatin and two masses of condensed chromatin (*ch*), basal knobs, are free of precipitates in an early pachytene nucleus. A synaptonemal complex is seen (arrow). A secondary nucleolus (*n*) shows a small amount of antimonate deposits. Clusters of precipitates are observed between the dense chromatin masses. Pyroantimonate fixation. Stained with uranyl acetate and lead citrate. Scale mark, 1 μ. × 15,000.

FIGURE 9 Part of a spermatocyte nucleus at late pachytene showing absence of antimonate deposits in the elements of the sex pair (*XY*); axial element (arrow); associated round body (*). Some antimonate precipitate appears between areas of the decondensed chromatin. Pyroantimonate fixation. Stained with uranyl acetate and lead citrate. Scale mark, 1 μ. × 15,600.

FIGURE 10 This micrograph shows cation-antimonate precipitates mainly along the margins of meiotic chromosomes in two spermatocytes. Pyroantimonate fixation. Stained with uranyl acetate and lead citrate. Scale mark, 2 μ. × 5000.

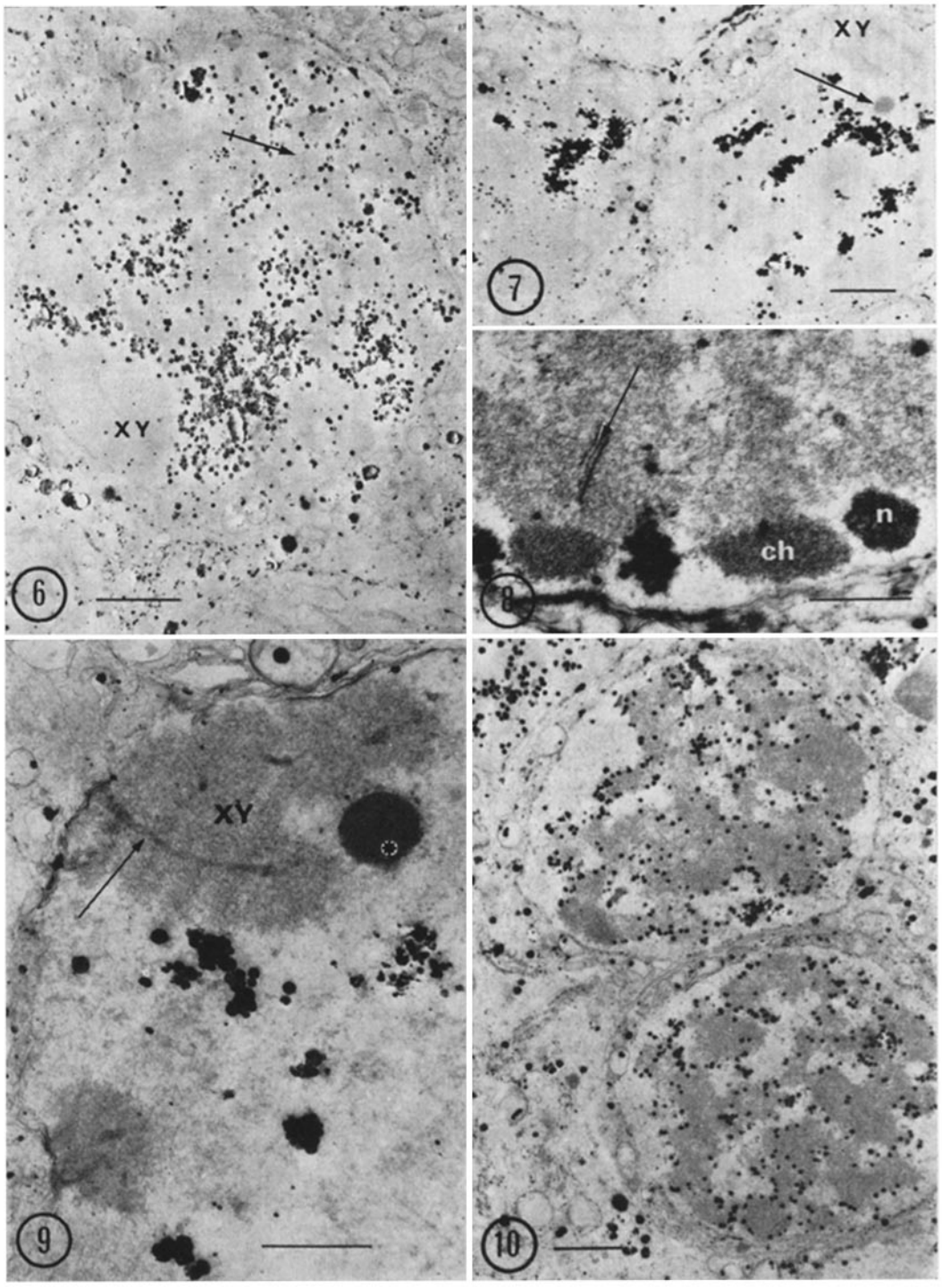
XY
6
XY
7
n
ch
8
XY
9
10

precipitate is very similar to the antimonate deposits distributed in the nucleoplasm. A comparison with glutaraldehyde-osmium tetroxide-fixed nuclei (Fig. 13) indicates that the coarser type of precipitate corresponds—in size and distribution—to the fibrillar and amorphous areas of the nucleolus (fibrillar centers, reference 23), whereas the granular component shows the finer type of antimonate deposit. Inactive chromatin—the condensed chromatin bodies—is free of precipitate (Fig. 12).

The cytoplasmic extensions of Sertoli cells apparently possess a higher amount of electron-opaque precipitates than the cytoplasm of germinal cells (Fig. 1).

DISCUSSION

The present observations in the mouse testis confirm and extend the previous ones made with the use of potassium pyroantimonate as a fixative for electron microscope and microprobe analysis (4). As to the chemical nature of antimonate precipitates, we rely principally on the microprobe evidence that the common tissue cations Mg^{++}, Ca^{++}, and Na^{+} are present in those precipitates. This particularly refers to the sites where relatively heavy electron-opaque deposits are evidenced, i.e., in nuclei and basement membranes (4). At present, the technique does not allow a distinction to be made between the different antimonate salts deposited in the tissue and does not indicate whether organic cations also are present in those deposits. A lighter electron opacity (or "staining" effect, reference 4) could be due to binding to unidentified reactive tissue groups; in fact, the striking property of the pyroantimonate anion as a fixative at the ultrastructural level must rely on this type of reaction (e.g., complexing with some carboxyl groups, reference 5).

In earlier work, the condensed chromatin was found generally free of antimonate precipitates (4–6); the same applies to the whole nuclei of mature spermatids (4, 31). It is difficult to envisage the reason why large amounts of soluble cations—if they exist associated with condensed chromatin—would escape the precipitating reagent, whereas the same cations precipitate at other sites within the nucleus. An artifactual redistribution due to displacement of diffusible ions certainly can be discarded in the case of nuclei of mature spermatids. The problem arises, therefore, whether inorganic cations are present at low concentrations in condensed chromatin (i.e., under the sensitivity of the antimonate test) or whether they exist in a firmly bound state (e.g., chelated) and not reactive to pyroantimonate anions.

Changes in the autosomal chromatin are observed that are related to different stages of the meiotic prophase. These events apparently are not related to antimonate distribution either, although at early to middle pachytene the precipitates appear to be located frequently at the edges of chromatin (Figs. 6 and 10). The meiotic prophase also shows the formation of special structures, the axial elements and synaptonemal complexes (24–26). One of the endings of the synaptonemal complexes against the nuclear membrane in mouse spermatocytes is surrounded by condensed chromatin called "basal knobs" (16); these basal knobs in the mouse and in the human are closely related to

FIGURE 11 Middle pachytene nucleus showing secondary nucleolus (*n*) of granular structure associated with a basal knob of dense chromatin having a synaptonemal complex (thick arrow). The sex pair (*XY*) with axial elements and granular portions of the main nucleolus (*gr*); clusters of interchromatin granules (*); perichromatin granules (thin arrows). Glutaraldehyde–osmium tetroxide fixation. Stained with uranyl acetate and lead citrate. Scale mark, 1 μ. × 12,000.

FIGURE 12 In the nucleus of a Sertoli cell the cation-antimonate deposits are dispersed in the nucleoplasm, and a few clusters of precipitates are also seen. In the nucleolus (*n*) the precipitates are concentrated in the amorphous and fibrillar areas; a finer precipitate delimits the nucleolus. Associated heterochromatin body, *cb*. Pyroantimonate fixation. Unstained. Scale mark, 1 μ. × 12,000.

FIGURE 13 A Sertoli cell nucleus fixed in glutaraldehyde–osmium tetroxide. The nucleolus (*n*) shows areas of associated amorphous and fibrillar components, similar in morphology to the antimonate deposition of Fig. 12. The nucleoplasm shows some large clusters of interchromatin granules (*). Associated chromatin body near the nucleolus, *cb*. Stained with uranyl acetate and lead citrate. Scale mark, 2 μ. × 8400.

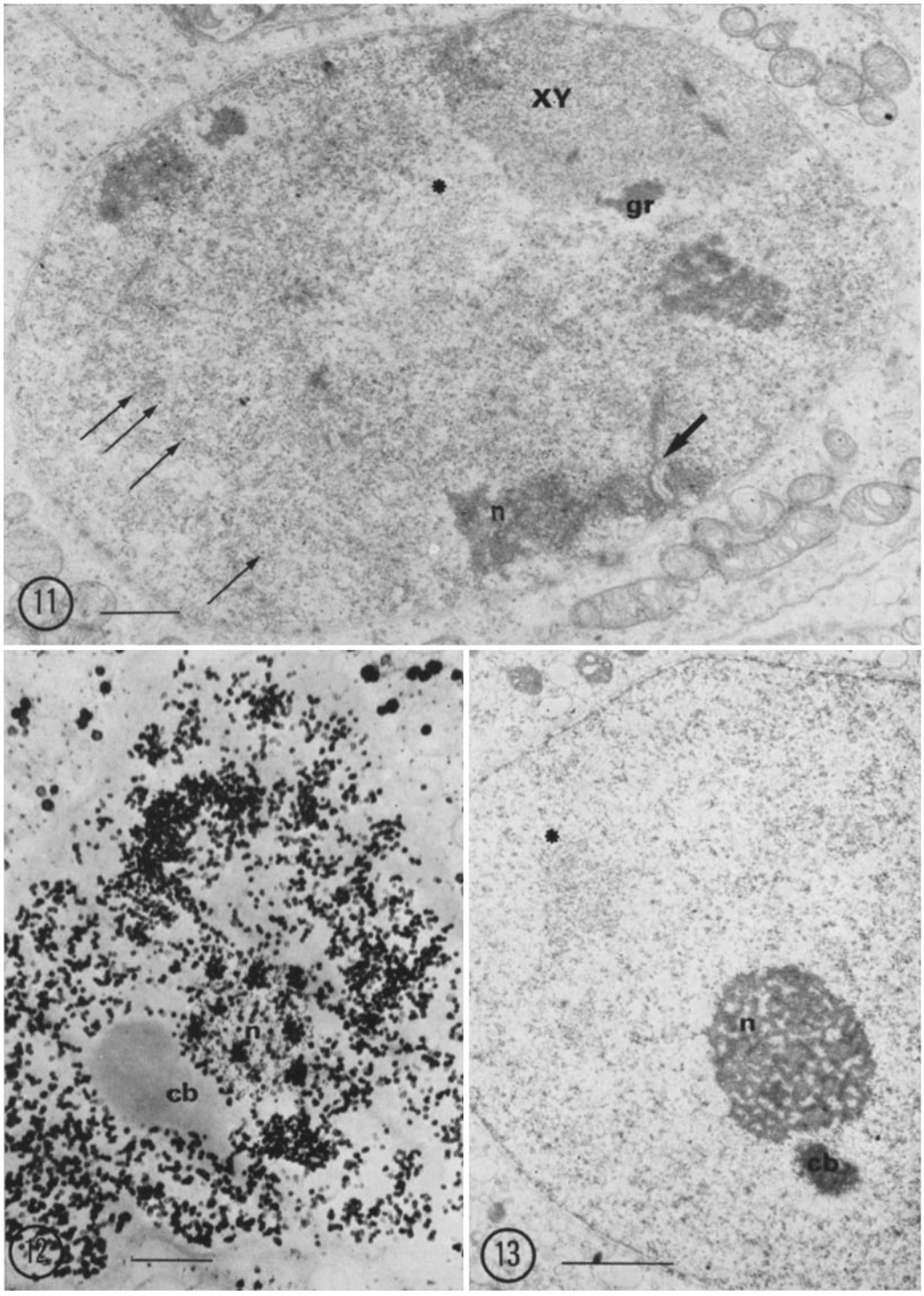
XY
gr
n
11
n
cb
12
n
cb
13

the formation of the so-called secondary nucleoli (10, 16, 27, 28). All these structures, with the probable exception of secondary nucleoli (Fig. 8), are devoid of antimonate precipitates.

The absence of antimonate deposits in the heterochromatin body which constitutes the sex pair could be related to the inactivation of the XY bivalent, as judged by the lack of incorporation of labeled RNA precursors (8, 9). The main nuclelous is associated with the sex pair (10). The ultrastructural characteristics of this nucleolus are not easily recognized after pyroantimonate fixation; in none of these structures is the presence of antimonate precipitates discernible. This stands in contrast with the finding in the nucleolus of Sertoli cells.

Cation Accumulation in the Nucleus and RNA Synthesis

The evidence presented here demonstrates that the presence of inorganic cations in the nucleus is related, at least partially, to the transcription process. This is indicated by: (*a*) in a given tissue an accumulation of cations occurs in the nucleus of those cells engaged in enhanced RNA synthetic activity. In the middle pachytene nuclei as opposed to earlier or later stages this seems particularly evident, as the spermatogenic process is a very regular one in the mouse (11); and (*b*) within a given cell the intranuclear sites of RNA synthesis—in the nucleoplasm and nucleolus—are also the sites of cation accumulation. Since RNA synthesis is due to the enzymic activity of RNA polymerases, and since this in turn is dependent on divalent cations plus a certain ionic strength (7), it seems evident to conclude that the selective inorganic cation accumulation observed in different cell types—as described in the present paper—is correlated mainly with the presence of RNA polymerases.

The nucleoplasmic types of RNA polymerases (7) require, besides a divalent cation, a high ionic strength for optimal activity. Inorganic cations are accumulated in the nucleoplasm (interchromatin localization) and at the border of the chromatin (perichromosomal localization). The last pattern appears in spermatocytes at those stages where an activation of autosomal chromosomes occurs, resulting in enhanced RNA synthesis. Fakan et al. (29) recently demonstrated that the very rapidly chromosomal or DNA-like RNA is seen at the border of condensed chromatin, in the region where perichromatin fibrils have been detected (30). Although the size of antimonate precipitates in the nuclei is too large to allow a precise localization, their perichromosomal distribution is evident in Fig. 10. These data provide indirect proof for the presence of RNA polymerases at the border of activated chromosomes.

Inorganic cations in the nucleoplasm are frequently accumulated in the form of patches which apparently are coincident with clusters of interchromatin granules. The same observation has been verified in immature spermatids (31) and in other mammalian tissues (in preparation). These data favor the suggestion that RNA polymerases are concentrated in the areas of interchromatin granules and may be responsible for the synthesis of a very slowly labeled RNA species present in the nucleoplasmic ribonucleoproteins (29).

The main type of nucleolar RNA polymerase (7) is dependent on a divalent cation and does not require a high ionic strength. Jacob et al. (32) reported that RNA polymerization by isolated nucleoli was dependent on two polymerase activities and that only one of them requires a high ionic strength. Inorganic cations are accumulated in the nucleolus of Sertoli cells preferentially in the fibrillar and/or amorphous areas (fibrillar centers, reference 23), i.e., at sites where intranucleolar transcription of the ribosomal precursor RNA is known to take place (33, 34). This peculiar type of antimonate distribution was also described in neuronal nucleoli by Spicer et al. (35, 36) who used a mixture of osmium tetroxide and potassium pyroantimonate. These data favor the suggestion that the nucleolar RNA polymerases are concentrated in the fibrillar and amorphous components of the nucleolus; it might be asked whether the areas of amorphous portions—which appear to be free of RNA (34)—represent foci of (excess?) RNA polymerase in these normally segregated types of nucleoli.

Besides RNA polymerases, other enzymes whose activity is dependent on inorganic cations have been detected in the nucleus (1). It is conceivable that some of these enzymes also might be located at sites of cation accumulation in the nucleoplasm and nucleolus (e.g., cf. reference 37 for nucleoside triphosphatases).

It should be mentioned here also that the inorganic cations in the living nuclei appear to be in a loosely "bound" form (1) and probably electrically neutralized with a large pool of inorganic orthophosphate anions (38).

In conclusion, we have visualized the inorganic salt accumulations which are expected to occur during transcription at different intranuclear sites in spermatogenic cells during the meiotic prophase and in Sertoli cells in the mouse testis. The extension and refinement of this technique should provide a new approach to the study of the functional significance of the presence of inorganic salts in the nucleus, particularly regarding the in vivo ionic conditions for RNA polymerase activity.

The authors wish to express their thanks to Professor R. E. Mancini for providing the facilities for this study. We gratefully acknowledge the outstanding assistance of Miss Estela L. Kirlis.

This investigation was supported by a grant from the Consejo Nacional de Investigaciones Científicas y Técnicas, Argentina and The Population Council, Inc., New York. Doctors Laura L. Tres and C. J. Tandler are established investigators in the C.N.I.C.T.

Received for publication 16 August 1971, and in revised form 18 January 1972.

REFERENCES

1. Siebert, G., and G. B. Humphrey. 1965. *Advan. Enzymol.* **27**:239.
2. Okazaki, K., K. H. Shull, and E. Farber. 1968. *J. Biol. Chem.* **243**:4661.
3. Siebert, G., and H. Langendorf. 1970. *Naturwissenschaften.* **57**:119.
4. Kierszenbaum, A. L., C. M. Libanati, and C. J. Tandler. 1971. *J. Cell Biol.* **48**:314.
5. Tandler, C. J., and A. L. Kierszenbaum. 1971. *J. Cell Biol.* **50**:830.
6. Tandler, C. J., C. M. Libanati, and C. A. Sanchis. 1970. *J. Cell Biol.* **45**:355.
7. Transcription of Genetic Material. 1970. Cold Spring Harbor Symposia on Quantitative Biology. **35**.
8. Monesi, V. 1964. *J. Cell Biol.* **22**:521.
9. Monesi, V. 1965. *Exp. Cell Res.* **39**:197.
10. Solari, A. J. 1969. *J. Ultrastruct. Res.* **27**:289.
11. Oakberg, E. F. 1956. *Amer. J. Anat.* **99**:391.
12. Fawcett, D. W., E. M. Eddy, and D. M. Phillips. 1970. *Biol. Reprod.* 2:129.
13. Solari, A. J. 1964. *Exp. Cell Res.* **36**:160.
14. Solari, A. J., and L. Tres. 1967. *Exp. Cell Res.* **47**:86.
15. Tres, L., and A. J. Solari. 1966. *Acta Physiol. Latinoamer.* **16**(Suppl. 1):129.
16. Woollam, D. H. M., and E. H. R. Ford. 1964. *J. Anat.* **98**:163.
17. Swift, H. 1963. *Exp. Cell Res. Suppl.* **9**:54.
18. Watson, M. L., and W. G. Aldridge. 1964. *J. Histochem. Cytochem.* **12**:96.
19. Monneron, A., and W. Bernhard. 1969. *J. Ultrastruct. Res.* **27**:266.
20. Moens, P. B. 1968. *Chromosoma.* **23**:418.
21. Callan, H. G., and J. H. Taylor. 1968. *J. Cell Sci.* **3**:615.
22. Kofman-Alfaro, S., and A. C. Chandley. 1970. *Chromosoma.* **31**:404.
23. Recher, L., J. Whitescarver, and L. J. Briggs. 1969. *J. Ultrastruct. Res.* **29**:1.
24. Moses, M. J. 1956. *J. Biophys. Biochem. Cytol.* **2**:215.
25. Moses, M. J. 1968. *Annu. Rev. Genet.* **2**:363.
26. Moses, M. J. 1969. *Genetics.* **61**(Suppl. 1):41.
27. Solari, A. J., and L. L. Tres. 1967. *Chromosoma.* **22**:16.
28. Solari, A. J., and L. L. Tres. 1970. *J. Cell Biol.* **45**:43.
29. Fakan, S., and W. Bernhard. 1971. *Exp. Cell Res.* **67**:129.
30. Petrov, P., and W. Bernhard. 1971. *J. Ultrastruct. Res.* **35**:386.
31. Kierszenbaum, A. L., L. L. Tres, and C. J. Tandler. 1972. *J. Cell Biol.* **53**:239.
32. Jacob, S. T., E. M. Sajdel, and H. N. Munro. 1968. *Biochim. Biophys. Acta.* **157**:421.
33. Granboulan, N., and P. Granboulan. 1965. *Exp. Cell Res.* **38**:604.
34. Busch, H., and K. Smetana. 1970. The Nucleolus. Academic Press Inc., New York.
35. Spicer, S. S., J. H. Hardin, and W. B. Greene. 1968. *J. Cell Biol.* **39**:216.
36. Hardin, J. H., and S. S. Spicer. 1970. *J. Ultrastruct. Res.* **31**:16.
37. Vorbrodt, A., and W. Bernhard. 1968. *J. Microsc.* **7**:195.
38. Tandler, C. J., and A. J. Solari. 1969. *J. Cell Biol.* **41**:91.